frontiers | Frontiers in Manufacturing Technology

TYPE Original Research
PUBLISHED 02 February 2023
DOI 10.3389/fmtec.2023.1104742

OPEN ACCESS

EDITED BY
Sangkee Min,
University of Wisconsin-Madison,
United States

REVIEWED BY
Mariusz Deja,
Gdansk University of Technology, Poland
Sajan Kapil,
Indian Institute of Technology Guwahati,
India

*CORRESPONDENCE
So Ito,
so.ito@pu-toyama.ac.jp

SPECIALTY SECTION
This article was submitted to Precision Engineering,
a section of the journal
Frontiers in Manufacturing Technology

RECEIVED 22 November 2022
ACCEPTED 02 January 2023
PUBLISHED 02 February 2023

CITATION
Aruga M, Ito S, Kato D, Matsumoto K and Kamiya K (2023), Investigation of probing repeatability inside a micro-hole by changing probe approach direction for a local surface interaction force detection type microprobe.
Front. Manuf. Technol. 3:1104742.
doi: 10.3389/fmtec.2023.1104742

Investigation of probing repeatability inside a micro-hole by changing probe approach direction for a local surface interaction force detection type microprobe

Masakazu Aruga, So Ito*, Daichi Kato, Kimihisa Matsumoto and Kazuhide Kamiya

Department of Intelligent Robotics, Faculty of Engineering, Toyama Prefectural University, Imizu, Japan

The inner diameter measurement of the micro-hole was performed by a tactile microprobing system using a method of the local surface interaction force detection. The inner diameter of the micro-hole was calculated by the least square method based on the probing coordinates obtained by a custom-made micro-coordinate measuring machine. The dispersion of the probing coordinates was investigated by changing the probe approaching direction with respect to the normal direction of the inner side of the micro-hole. During the probing inside the micro-hole, it was confirmed that the dispersion of the probing coordinates increased when the disagreement between the probe approaching direction and the normal direction of the micro-hole at the measured point became large. The influence of the dispersion of the probing coordinates was evaluated through the uncertainty analysis of the inner diameter measurement. It was revealed that the uncertainty of the inner diameter measurement could be improved when limiting the disagreement between the probe approaching direction and the normal direction of the micro-hole to within ±pi/4 rad.

KEYWORDS

microprobe, CMM, inner diameter, laser processing machining, surface interaction force

1 Introduction

Small holes with inner diameters of less than 0.5 mm, which are often called micro-holes (Masuzawa, et al., 1993), are widely used as inkjet printer nozzles, internal combustion engine fuel injector spray holes, and pinholes in optical systems, and in three-dimensional electronic circuit packaging wiring (Wilson, 1995; Kao and Shih, 2007; Sato, et al., 2020). The fabrication of micro-holes on the surface of a workpiece to control the hydrophobicity (Cai, et al., 2018) and tribological properties (Song, et al., 2018) of the surface have also been studied. Therefore, micro-hole fabrication is an important technique in manufacturing. Various fabrication methods, such as miniaturized machine tools (Aziz, et al., 2012; Li, et al., 2021), electrical discharge machining (EDM) (Tong, et al., 2013) and electrochemical discharge machining (ECDM) (Saranya and Sankar, 2018; Arab, et al., 2019), have been proposed to realize micro-holes with fine inner diameters and high form accuracy. Laser processing machining, which includes laser drilling, is also widely used to form micro-holes with high aspect ratios, and can be used to form micro-holes in various materials such as glass (Sato, et al., 2020), metals (Sato, et al., 2020), alloys (Gupta, et al., 2016; Marimuthu et al., 2019), silicon carbide (Krüger, et al., 2007), and glass epoxy. Furthermore, the machining time in the laser drilling is generally shorter

than that in machining or EDM/ECDM, and many micro-holes can be fabricated in a short time without tool wear. However, the inner diameters of the micro-holes fabricated by laser drilling are often ununiform along the depth direction, and the micro-holes often have a tapered or barrel cross-sectional shape (Krüger, et al., 2007; Gupta, et al., 2016; Marimuthu et al., 2019). Consequently, the inner diameters of the micro-holes do not necessarily coincide with the opening diameters at the surface. The inner diameter measurement of micro-holes has been performed by scanning electron microscopy (SEM) observation of split micro-hole specimens. This is a destructive inspection, and the sample preparation is time-consuming. In addition, it is difficult to calculate geometrical tolerances, such as the straightness of the micro-holes, from measurements of the inner diameters through SEM observations. Optical method represented by MLP-3 (Mitaka Kohki Co., Ltd.) can measure the inside of the hole non-destructively, however, there is a trade-off between increased measurable depth and resolution.

Coordinate measuring machines (CMMs) that employ tactile probing system provide a practical means of measuring complex dimensions, including the inner diameter and depths of micro-holes (Weckenmann, et al., 2004; Claverley and Leach, 2015). In recent years, CMMs using microprobes incorporating probe tip balls with diameters of less than 1 mm have been developed (Weckenmann, et al., 2006; Weckenmann and Schuler, 2011; Thalmann, et al., 2016). Because the position of the inner wall can be directly determined by inserting the tip ball of the microprobe inside the micro-hole, the inner diameter and form of the micro-hole can be measured non-destructively (Murakami, et al., 2014; Elfurjani, et al., 2016). In CMMs that uses tactile probing systems, the deformation of the measured point or probe tip ball due to the measurement force of the tactile probe causes measurement errors (Weckenmann, et al., 2004; Weckenmann and Schuler, 2011). Therefore, probing systems with vibrating micro-styli have been developed to reduce the measurement force (Claverley and Leach, 2010; Bos, 2011). The probing systems with the vibrating micro-styli detect the change in the vibration state of the micro-styli due to the intermittent contact of the probe tip or the interaction force, and the vibration changes are used as a trigger signal for probing. In the authors' previous works, probing was performed by using a vibrating micro-stylus to detect the local surface interaction force near the surface of the measured workpieces (Ito, et al., 2016a; Ito et al., 2016b; Chen, et al., 2016). The stylus vibration along the main axis of the stylus shaft in the microprobing system was employed to detect the local surface interaction force in all directions around the main axis (Ito, et al., 2020). However, in probing on a cylindrical pin gauge, the dispersion of the probing coordinates increased as the disagreement between the probe approaching direction and the normal direction of the measured object became larger. As the similar studies, the precision measurements of the vertical side walls of the microstructures have been performed using the microprobing systems (Li, et al., 2018; Metz, et al., 2019; Dai, et al., 2020). In these studies, the probing was performed on the vertical flat planes, therefore, probing repeatability due to difference of the probe approaching directions was not focused.

In this study, the inner diameter measurement of the micro-hole was conducted by using a microprobing system with a method of local surface interaction force detection. A micro-stylus with a tip ball of less than 50 μm in diameter was fabricated from a capillary glass tube for probing inside the micro-hole with a diameter of less than 80 μm. The probing characteristic derived from the disagreement between the probe approaching direction and normal direction of the micro-hole was evaluated as the repeatability of the probing coordinates. The inner diameter of the micro-hole was calculated by applying the least squares method to the probing coordinates. The influence of the probing repeatability on the inner diameter measurement due to the difference in probe approaching direction was estimated as measurement uncertainty.

2 Experimental method

2.1 Microprobing system

The tip of the microprobe was formed into a spherical shape owing to maintain a uniform shape in all direction inside the micro-hole. A micro-stylus with an aspherical tip was fabricated from a glass capillary tube. After the glass capillary tube was sharpened through a thermal pulling process, the sharpened edge of the glass tube was melted using a platinum heater in a microforge (MF2, NARISHIGE). The edge of the melted glass tube formed into a sphere spontaneously because of surface tension. Figure 1A shows a microphotograph of the spherical micro-stylus tip fabricated from a glass capillary tube. The diameter of the stylus tip ball was measured by an optical microscope (NH-3S, Mitaka Kohki) with lateral resolution of 0.1 μm. The diameter of the probe tip ball, D_p, was measured to be 39.1 ± 0.2 μm. According to the previous research (Ito et al., 2016a), measurement uncertainties due to motion errors of the probe positioning stages can be reduced when the difference between the aperture dimension and the probe tip ball diameter is small. The micro-stylus formed by heat drawing has a tapered shape. An effective length of a micro-stylus is defined as the length from the stylus tip to the point where the stylus diameter equals the probe tip sphere diameter. The effective length of the micro-stylus used in this study was evaluated to be 2.0 mm. During the probing, the tip of the micro-stylus is vibrated parallel to the inner side wall to detect the surface of the micro-hole. Figure 1B shows a probe vibration sensor made of tuning fork quartz crystal resonator (TF-QCR). The vibration of the micro-stylus can be detected through the piezoelectric effect of the quartz crystal. The micro-stylus is fixed on one beam of the TF-QCR using glue. The TF-QCR with the micro-stylus are vibrated in the Z direction at resonance frequency by a PZT transducer. The nominal resonance frequency of the TF-QCR is 32.768 kHz.

When the tip of the vibrating microprobe is coming close to the surface of the workpiece, the resonance frequency of the microprobe vibration is changed due to the local surface interaction force. The local surface interaction force is roughly divided into repulsive force and attractive force. The local repulsive force is mainly caused by contact or intermittent contact between the tip of the vibrating microprobe and the surface of the workpiece (Goj, et al., 2014). The local attractive force is derived from various non-contact interaction such as van deer Waals force, electrostatic force, and adhesion force of the surface thin water layer. When the local repulsive force acts the tip of the microprobe, the resonance frequency of the microprobe vibration is increased. On the other hand, the resonance frequency of the microprobe is decreased when the local attractive force is applied to the tip of the vibrating microprobe. In this study, the absolute value of the resonance

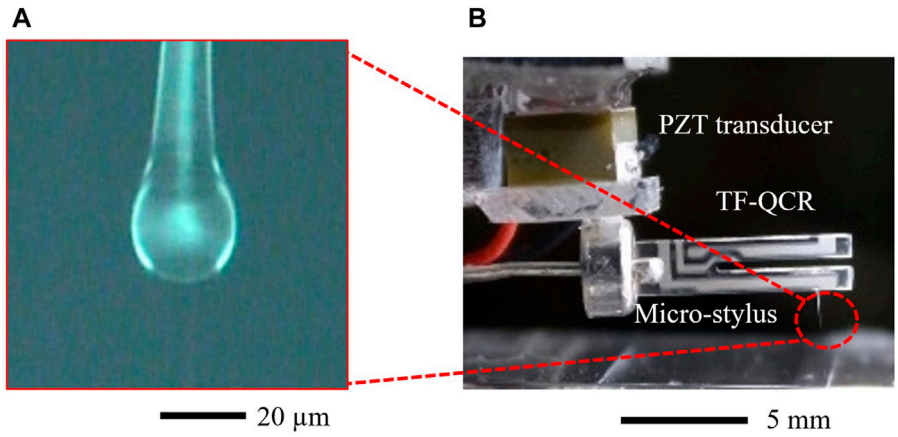

FIGURE 1
Photograph of microprobe used in this study. **(A)** Microphotograph of a spherical tip of a micro-stylus. **(B)** Probe vibration sensor made of tuning fork quartz crystal resonator (TF-QCR).

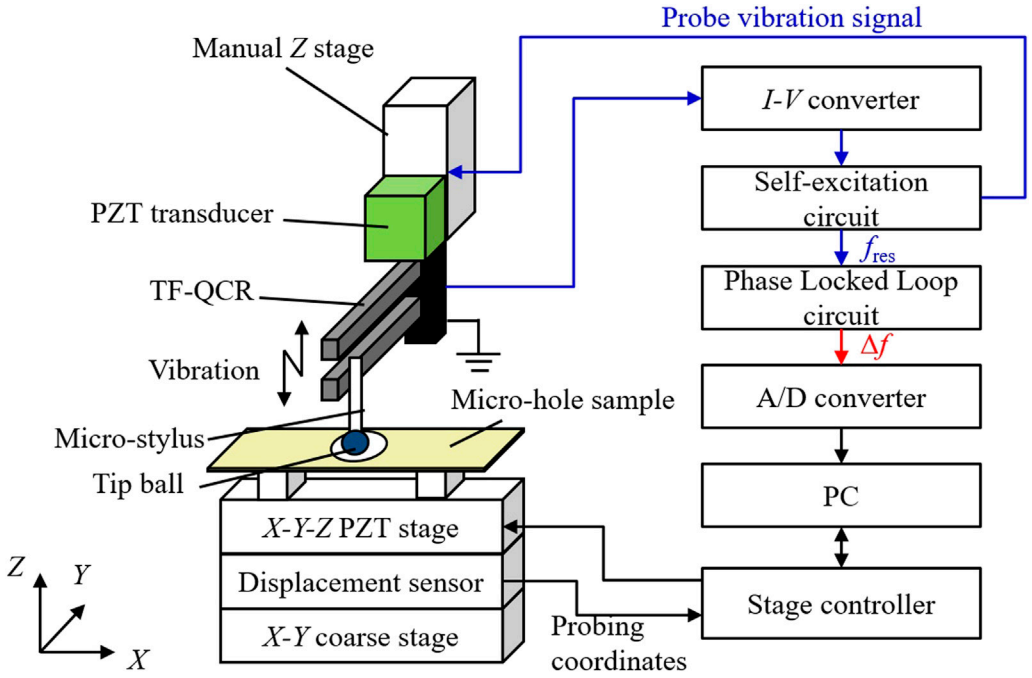

FIGURE 2
Configuration of microprobing system.

frequency shift amount of the microprobe vibration is detected and utilized as a trigger signal for the probing. Figure 2 shows the configuration of the prototype microprobing system. The vibration signal from the TF-QCR is converted and amplified by a custom made current-to-voltage conversion circuit (*I-V* converter). The resonance frequency of the microprobe vibration f_{res} is maintained by a self-excitation phase shifter circuit in a commercially available oscillation controller (OC4/RC4, Nanonis). The oscillation controller is designed for frequency modulation (FM) detection in dynamic-mode atomic force microscopes (AFMs) and maintains constant frequency and constant amplitude of the microprobe vibration by closed-loop control. The shift amount of the resonance frequency of the microprobe vibration due to the local surface interaction force, Δf, is detected by a phase-locked loop (PLL) circuit in the oscillation controller, which outputs as DC voltage signal that corresponds to the amount of frequency shift. The DC signal, which is called the Δf signal, is fed into an analog-to-digital (A/D) converter (USB-6003, National Instruments) connected to a personal computer (PC) as the trigger signal for probing. Probing was performed by moving the workpiece surface so that the surface approaches the tip of the microprobe to avoid noise caused by mechanical vibration during the movement of the probe (Weckenmann, et al., 2006).

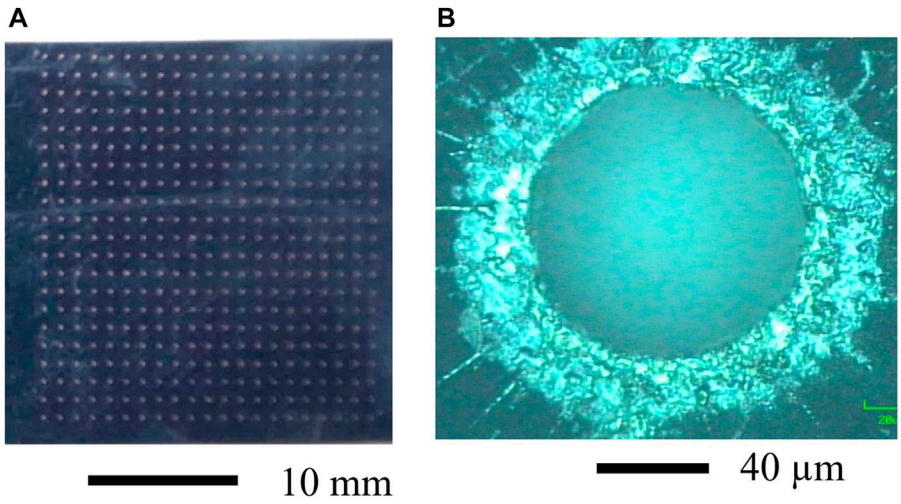

FIGURE 3
Microphotographs of micro-holes. **(A)** Micro-hole array on the substrate surface **(B)** Microphotograph of a micro-hole.

The measured workpiece was placed on the sample holder, which was a height of 25 mm, and mounted on a moving table of the PZT-driven *X-Y-Z* fine positioning stage (SFS-H60XYZ, SIGMAKOKI). The displacement of the stage table was measured by the built-in capacitive-type displacement sensors, and the position of the moving table was maintained by closed-loop control. The displacement sensors were installed 30 mm below the top of the stage table. The stroke and resolution of the fine positioning stage were 85 μm and 10 nm in each direction. The stage displacement when Δf became larger than a certain threshold value was employed as the probing coordinate. To align the micro-holes on the measured workpiece and the tip of the microprobe, the fine positioning stage was mounted on the moving table of a *XY* coarse positioning stage (SGSP-20-35, SIGMAKOKI) driven by stepper motors. The stroke and resolution of the coarse positioning stages were 35 mm and 2 μm, respectively. The micro-hole and the tip ball of the microprobe were aligned using the coarse positioning stage and two optical microscopes which were used to observe from the *X* and *Y* directions, simultaneously. Figure 3 shows microphotographs of micro-holes. In this study, a sample of blind micro-hole laser-processed on a copper/glass-epoxy/copper substrate was used. The nominal diameter of the micro-hole aperture was 80 μm, the axial depth of the micro-hole was 55 μm.

2.2 Calculation of micro-hole diameter from probing coordinates

To calculate the inner diameter of the micro-hole based on the acquired probing coordinates, the least squares method was introduced. Although the *X-Y-Z* PZT stage of the microprobing system could move along the *X*, *Y*, and *Z*-axes, the *Z* coordinate of the positioning stage was held constant during the probing inside the micro-hole. Therefore, the radius, r, and center coordinate, $c(a, b)$, of the approximated circle of the probing coordinates are calculated from the probing coordinates in the *X* and *Y* directions. The distance L_i between the arbitrary probing coordinates $p_i(x_i, y_i)$ and an approximated circle of radius r can be expressed as,

$$L_i = \sqrt{(x_i - a)^2 + (y_i - b)^2} - r. \tag{1}$$

In the least square method, $c(a, b)$ and r are calculated using the following formula to minimize the sum of squares of L_i:

$$\begin{pmatrix} \sum_{i=1}^{n} x_i^2 & \sum_{i=1}^{n} x_i y_i & \sum_{i=1}^{n} x_i \\ \sum_{i=1}^{n} x_i y_i & \sum_{i=1}^{n} y_i^2 & \sum_{i=1}^{n} y_i \\ \sum_{i=1}^{n} x_i & \sum_{i=1}^{n} y_i & \sum_{i=1}^{n} 1 \end{pmatrix} \begin{pmatrix} A \\ B \\ C \end{pmatrix} = \begin{pmatrix} -\sum_{i=1}^{n} (x_i^3 + x_i y_i^2) \\ -\sum_{i=1}^{n} (x_i^2 y_i + y_i^3) \\ -\sum_{i=1}^{n} (x_i^2 + y_i^2) \end{pmatrix} \tag{2}$$

where n is the number of probing coordinates, and A, B, and C are defined as follows:

$$A = -2a, \tag{3}$$

$$B = -2b, \tag{4}$$

$$C = a^2 + b^2 - r^2. \tag{5}$$

The center coordinate, $c(a, b)$ and radius of the approximated circle, r, can be calculated by solving Eqs 1–5. However, the probing coordinates acquired by the displacement sensors built into the fine positioning stages were the center coordinates of the probe tip ball, not the coordinates of the contact point between the probe tip and the measured workpiece. Therefore, inner diameter of the micro-hole was calculated by adding the diameter of the probe tip ball. The inner diameter of the micro-hole, was calculated by the following equation.

$$D = 2r + D_p, \tag{6}$$

where, D_p is the diameter of microprobe tip ball.

3 Experimental results and discussion

3.1 Measurement procedure

In the microprobing system used in this study, probing was performed by moving the micro-hole sample using the fine positioning stage. Therefore, the position of the microprobe was

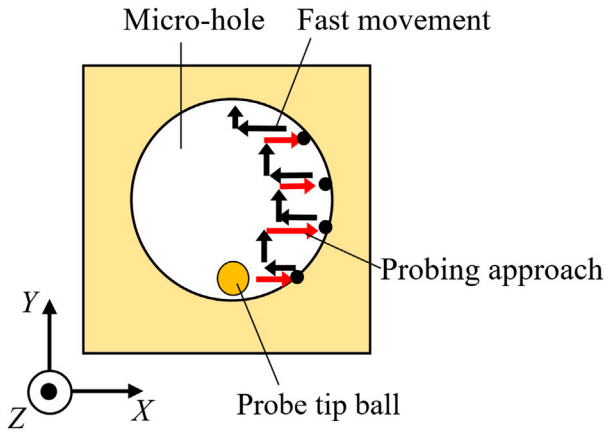

FIGURE 4
Trajectory of the probe tip in the micro-hole during the probing in +*X*-direction.

stationary during the actual measurement. However, for simplicity, the procedure is explained here using the relative motion of the microprobe tip. The movement of the micro-hole sample in the −*X* direction by the fine positioning stage corresponds to the relative movement of the microprobe in the +*X* direction, which is henceforth referred to as probing in the +*X* direction.

There are two methods for measuring the inner diameter of a hole using a tactile probing system. One is to bring the probe tip closer along the normal direction from the center of the hole. This method has been widely employed for commercially available macroscopic CMMs. However, it requires pre-measurement to calculate the center position of the hole. Therefore, the same hole must be measured at least twice, so it is time-consuming way. Another method is to move the probe in the *XY* direction along the moving axis of the fine positioning stages. Since this method can start to measure from any position inside the hole, the inner diameter can be calculated by one set of measurement. However, the probe approach direction does not always coincide with the normal direction of the micro-hole. The influence of disagreement between the probe approaching direction and normal direction of the micro-hole on the repeatability of probing was investigated. Figure 4 shows a schematic diagram of the trajectory of the probe tip in the micro-hole during the probing in the case of +*X* direction. To determine the surface position inside the micro-hole, the microprobe was moved in +*X* direction in steps of 10 nm per second. The microprobe coordinates in the *Y* and *Z* directions were kept constant *via* closed-loop control during probing in the +*X* direction. When the absolute value of the frequency shift Δ*f* of the probe vibration exceeded a given threshold, the probe position is recorded as the probing coordinates. Probing was repeated five times at the same *Y* position. Then, the microprobe was then moved 5 μm in the +*Y* direction, and the probing in the +*X* direction was repeated in a similar manner. Probing in the −*Y* direction was conducted in the same condition. As mentioned in Section 2.2, the center of the approximated circle of probing coordinates can be calculated by the least square method. Figure 5 shows a schematic of disagreement between the probe approach direction and normal direction of the micro-hole. The disagreement was defined as the angle, between the probe approach direction and the normal direction of the micro-hole.

3.2 Probing repeatability and calculation of inner diameter

The probing inside the micro-hole was conducted at the depth of 30 μm from the surface of the substrate. The resonance frequency of the microprobe vibration was 32.331 kHz, and the threshold of Δ*f* for the probing was set to 0.38 Hz. Blue plots in Figure 6 indicate the average values of probing coordinates repeated five times at the same location obtained by moving the probe tip closer to the inner wall of the micro-hole from the ±*X* directions. The error bars in Figure 6 show the maximum and minimum probing coordinates along the *X* direction. After probing in the +*X* direction, probing in the −*X* direction was immediately conducted on the opposite inner wall of the micro-hole. Since only the fine positioning stage was moved during the probing inside the micro-hole, the probing coordinates were calculated from the displacement of the fine positioning stages. The

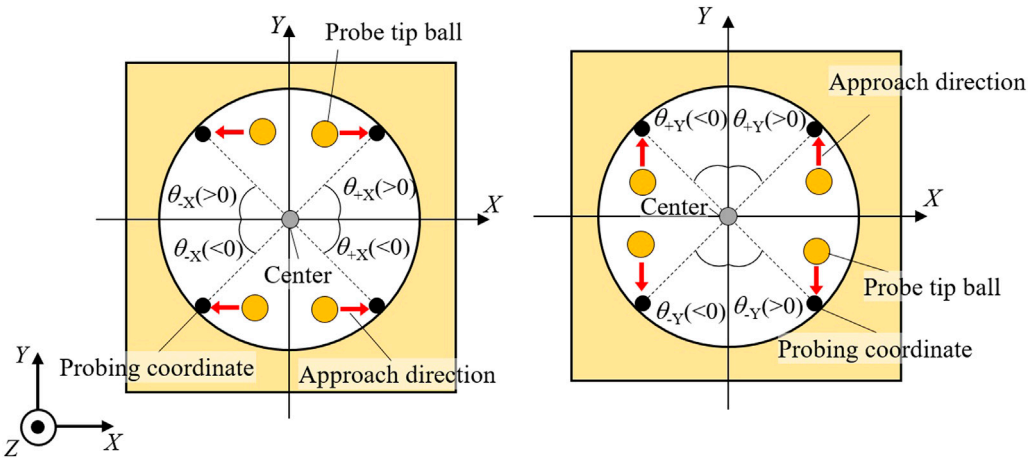

FIGURE 5
Schematic of disagreement of normal direction.

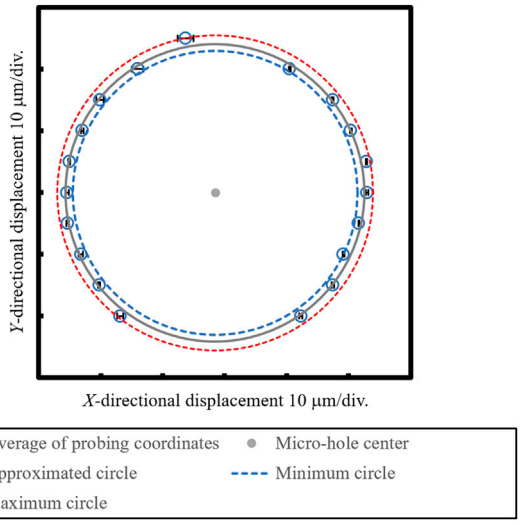

FIGURE 6
Probing coordinates inside the micro-hole in the *X*-direction.

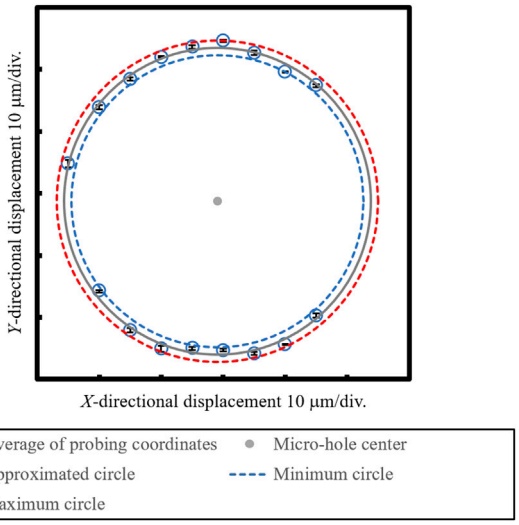

FIGURE 8
Probing coordinates inside the micro-hole in the *Y*-direction.

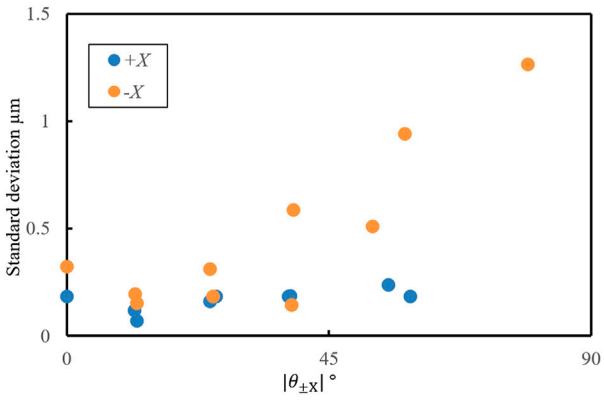

FIGURE 7
Relationship between the disagreement θ_X with the normal direction of the micro-hole and the standard deviation of the probing coordinates along the *X*-direction.

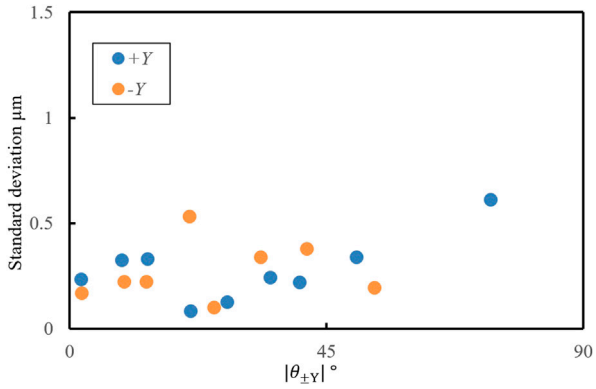

FIGURE 9
Relationship between the disagreement θ_Y with the normal direction of the micro-hole and the standard deviation of the probing coordinates along the *Y*-direction.

gray line and plot shown in Figure 6 are the approximated circle and center coordinate of the probing coordinates calculated by the least square method. The diameter of the approximated circle was calculated to be 48.2 μm, therefore, inner diameter of the micro-hole was evaluated to be 87.3 μm. The dashed lines in Figure 6 shows the minimum circumscribed circle and the maximum inscribed circle calculated from the average value of the *X*-directional coordinates at each probing position. The difference in radius between the minimum circumscribed circle and the maximum inscribed circle is evaluated to be 2.51 μm. Although the radius difference between the minimum circumscribed circle and the maximum inscribed circle is varies depending on the sphericity of the tip ball of the microprobe and the roundness of the micro-hole, it is also affected by the repeatability of the probing coordinates. Consequently, it is expected that the radius difference will decrease with the improvement of the probing repeatability. Figure 7 shows the relationship between the disagreement in $|\theta_{\pm X}|$ with the normal direction of the micro-hole and the standard deviation of the *X* coordinates of the probing positions. The maximum standard deviation in the $+X$ direction was 0.24 μm at $|\theta_{+X}|$ of 55.23°. Similarly, the maximum standard deviation in the $-X$ direction was 1.26 μm at $|\theta_{-X}|$ of 79.2°. The correlation coefficients of the standard deviations of the probing coordinates for the absolute values of the disagreement in $|\theta_{+X}|$ and $|\theta_{-X}|$ are calculated to be 0.605 and 0.840, respectively. Therefore, it was confirmed that the standard deviation of the probing coordinates tended to increase with the increase of $|\theta_{\pm X}|$.

Blue plots in Figure 8 shows the averaged probing coordinates repeated five times at the same location obtained by moving the probe tip closer to the inner wall of the same micro-hole from the $\pm Y$ directions. The error bars in Figure 8 show the maximum and minimum probing coordinates along the *Y* direction. The gray line and plot shown in Figure 8 indicate the approximated circle and center

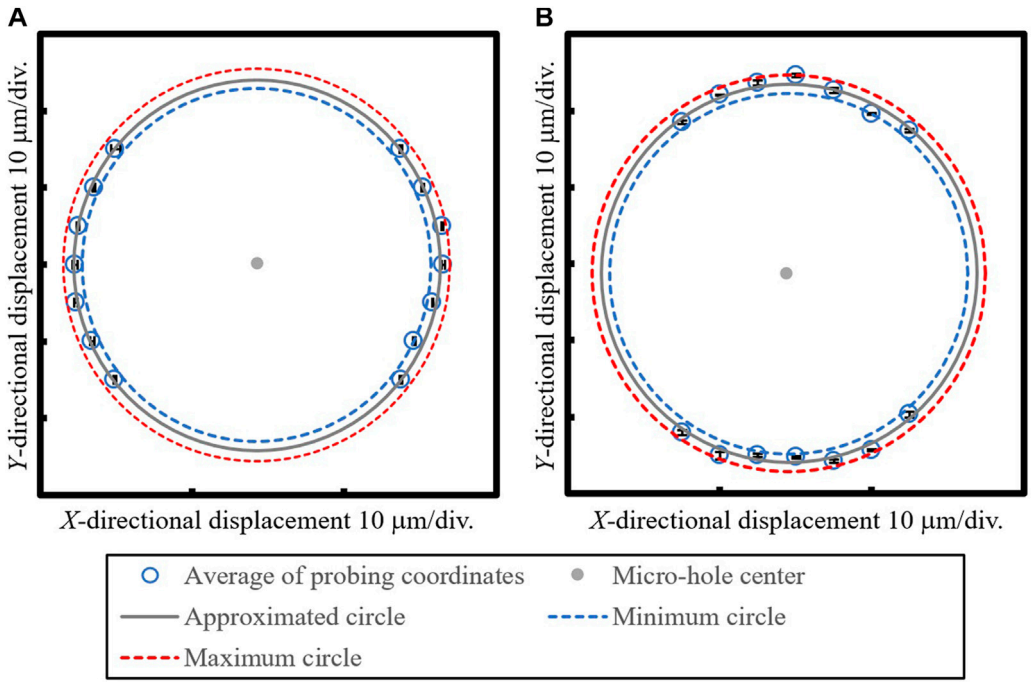

FIGURE 10
Probing coordinates inside the micro-hole in the *X* and *Y*-direction within range satisfying $|\theta_{\pm X}|$ <45°, and $|\theta_{\pm Y}|$ <45°. **(A)** Probing coordinates inside the micro-hole in the *X*-direction. **(B)** Probing coordinates inside the micro-hole in the *Y*-direction.

coordinate of the probing coordinates calculated by the least square method. The diameter of the approximated circle was calculated to be 49.4 μm, therefore, inner diameter of the micro-hole was evaluated to be 88.5 μm. The dashed lines in Figure 8 shows the minimum circumscribed circle and the maximum inscribed circle calculated from the average value of the *Y*-directional coordinates at each probing position. The difference in radius between the minimum circumscribed circle and the maximum inscribed circle is evaluated to be 2.35 μm. Figure 9 shows the relationship between the disagreement $|\theta_{\pm Y}|$ with the normal direction of the micro-hole and the standard deviation of the *Y* coordinates of the probing positions. The maximum standard deviation in the $+Y$ direction was 0.61 μm at $|\theta_{+Y}|$ of 75.80°. Similarly, the maximum standard deviation in the $-Y$ direction was 0.53 μm at $|\theta_{-Y}|$ of 20.89°. In the $+Y$ direction, the correlation coefficient of the standard deviation of the probing coordinates for the absolute value of the disagreement in $|\theta_{+Y}|$ is calculated to be 0.614, so an increasing tendency of the standard deviation due to the disagreement in $|\theta_{+Y}|$ is confirmed. On the other hand, the correlation coefficient of the disagreement in $|\theta_{-Y}|$ is calculated to be 0.162, and the correlation is not found.

In order to perform probing in all directions around the *Z*-axis in the micro-hole, $|\theta_{\pm X}|$ and $|\theta_{\pm Y}|$ have to be set to 45° and more. As the absolute value of the disagreement between the probe approaching direction and the normal direction of the measured micro-hole, the standard deviations of the probing coordinates tend to be increased, as shown in Figures 7, 9. In order to perform probing in all directions around the *Z*-axis in the micro-hole, $|\theta_{\pm X}|$ and $|\theta_{\pm Y}|$ have to be set to 45° at least. Therefore, the probing coordinates with the disagreement of $|\theta_{\pm X}|$ and $|\theta_{\pm Y}|$ within 45° are adopted, and the inner diameter of the micro-hole is calculated again. Blue plots in Figure 10 shows the averaged probing coordinates inside the micro-hole in the *X* and *Y*-direction within range satisfying $|\theta_{\pm X}|$ <45°, and $|\theta_{\pm Y}|$ <45°. Figure 10A shows the probing result in *X*-direction, and the diameters of the approximated circle and micro-hole are recalculated to be 48.0 μm and 87.1 μm, respectively. The difference in radius between the minimum circumscribed circle and the maximum inscribed circle of the approximated circle is evaluated to be 1.80 μm, and it become smaller than that of shown in Figure 6. Similarly, Figure 10B shows the probing result in *Y*-direction, and the diameters of the approximated circle and micro-hole are recalculated to be 49.6 μm and 88.7 μm, respectively. The difference in radius between the minimum circumscribed circle and the maximum inscribed circle of the approximated circle is evaluated to be 2.22 μm, and it becomes smaller than that of shown in Figure 8. The difference in diameter of the micro-hole in the *X* and *Y* directions may be caused by the distortion of the micro-hole and the probe tip ball. On the other hand, it is confirmed that the repeatability of the probing can be improved by limiting the disagreement between the probe approaching direction and the normal direction of the measured micro-hole.

3.3 Uncertainty analysis of inner diameter measurement

To evaluate the accuracy of the measurement of the micro-hole inner diameter, *D*, uncertainty analysis was carried out for each of the terms in Eq. 6 based on GUM (ISO *Guide to the Expression of Uncertainty in Measurement*) (JCGM 100, 2008). Table 1 shows a summary of the uncertainty budget for the measurement of the micro-hole inner diameter. Room temperature and its stability during the measurement of the micro-hole was measured to be 20°C ± 2°C. The

TABLE 1 Uncertainty budget (unit: nm).

Source of uncertainty	Symbol	Type	Value	Standard uncertainty
Uncertainty of probe tip diameter	u_{tip}		-	202.1
Resolution of optical microscope	u_{res_OM}	B	100	28.9
Diameter measurement of probe tip	u_{tip_dia}	A	400	200.0
Thermal effect (probe tip diameter)	$u_{tip\ thermal}$	B	0.5	0.1
Uncertainty of probing	$u_{probing}$		-	283.2
Repeatability of probing	$u_{rep\_probing}$	A	584	261.3
Positioning error (*X*-PZT stage)	$u_{X\_position}$	B	10	5.8
Positioning error (*Y*-PZT stage)	$u_{Y\_position}$	B	10	5.8
Abbe error (*X*-PZT stage)	u_{X_abbe}	B	133.3	77.0
Abbe error (*Y*-PZT stage)	u_{Y_abbe}	B	133.3	77.0
Uncertainty of micro-hole	u_{sample}		-	1.4
Thermal effect of micro-hole diameter	$u_{thermal\_hole\_dia}$	B	4.9	1.4
Expanded uncertainty (with a coverage factor $k = 2$)	U		-	695.8

combined standard uncertainty of "D_p" in Eq. 6 is defined as u_{tip}. Since the diameter of the probe tip ball was measured by the optical microscope with a horizontal resolution of 100 nm, the standard uncertainty of the measurement of the probe tip ball dimeter was estimated to be 28.9 nm from half width of the lateral resolution of the optical microscope. The measurement of the probe tip diameter was repeated twice in two orthogonal directions within the field of view of the optical microscope. Therefore, the repeatability of the diameter measurement of the probe tip, $u_{tip\ dia}$, was calculated to be 200 nm based on the error range of the probe tip diameter measurements. The thermal effect on the probe tip ball diameter, $u_{tip\ thermal}$, was evaluated from the thermal expansion coefficient of the probe material and the temperature change during the measurement. Thermal expansion coefficient of the probe tip ball, which made of borosilicate glass, is 3.25×10^{-6}/K. According to the temperature variation during the measurement mentioned above, $u_{tip\ thermal}$ was calculated to be 0.1 nm, which was ignored in Table 1. Consequently, the uncertainty of probe tip diameter u_{tip} is evaluated to be 202.1 nm.

Since "$2r$" in Eq. 6 is calculated by applying the least square method to the probing coordinates, the combined uncertainty of "r" is defined as $u_{probing}$. The standard uncertainty of the probing is calculated based on the standard deviation of the probing coordinate obtained inside the micro-hole. Within the measurement range $|\theta_{\pm X}|$ and $|\theta_{\pm Y}|$ of 45°, the maximum standard deviation of the probing coordinates at the same position was evaluated to be 0.58 mm at $\theta_{-X} = 39.0°$. The number of probing was set to be 5, and the standard uncertainty of the repeatability of the probing was calculated to be 261.3 nm. The probing coordinates are measured by the capacitive-type displacement sensors built into a closed-loop controlled PZT-driven fine positioning *XY* stages. Because positioning accuracy of the fine positioning *XY* stages are 10 nm, the standard uncertainty due to the positioning accuracy of the probing coordinates are evaluated to be 5.8 nm in *X* and *Y*-directions, respectively. There is an offset between the measuring axes of the capacitive displacement sensors in the fine positioning stage and the tip of the microprobe. Therefore, it does not satisfy Abbe's principle. The tilting errors of the stage table around the *X* and *Y*-axes of the fine positioning stage are called rolling and pitching in this study, and the pitching and rolling was estimated to be 0.5″, respectively. The offset from the displacement sensor in the fine positioning stages to the tip of the microprobe is 55 mm, and the Abbe error was calculated to be 133 nm. Consequently, the standard uncertainty derived from the Abbe error of the microprobe was estimated to be 77 nm. Consequently, the uncertainty of probing $u_{probing}$ is evaluated to be 283.2 nm.

The inner diameter of micro-hole varies with room temperature. Thermal expansion coefficient of the glass epoxy resin with micro-holes is 1.4×10^{-5}/K. According to the room temperature stability during the measurement, the standard uncertainty of the inner diameter of the micro-hole is calculated to be 1.4 nm. All the type B uncertainty sources were assumed to have a rectangular probability distribution with a coverage factor of $\sqrt{3}$. As a result, the expanded uncertainty U of the micro-hole inner diameter measurement was estimated to be 695.8 nm ($k = 2$).

4 Conclusion

The inner diameter of a micro-hole was measured by a microprobing system using a method of local surface interaction force detection. The probing was performed inside a micro-hole, and the inner diameter of the micro-hole was calculated by applying the least squares method for a circle to the probing coordinates and probe tip diameter. Consequently, the measurement of inner diameter of the micro-hole was achieved non-destructively. Although the probing coordinates at the interior of the micro-hole could be detected with sub-micrometric repeatability, deterioration of the probing repeatability due to the disagreement between the probe approaching direction and normal direction of the micro-hole was verified. It was possible to reduce the influence of the dispersion of the probing coordinates by limiting the disagreement of the probe approaching direction with respect to the

normal direction of the micro-hole. This method will be applicable to other inner shapes, however, the measurable shapes and dimensions, especially the measurable depth, is limited by the effective length of the microprobe stylus. Therefore, elongation of the micro stylus will expand the applicability of this method. The expanded uncertainty in the inner diameter measurement of the micro-hole was estimated to be 695.8 nm (k = 2), and one of the main sources of uncertainty was the repeatability of the probing. The other source of uncertainty was the measurement of the probe tip ball diameter, so the precision measurement and calibration of the probe tip diameter will become a future issue. In addition, three-dimensional measurements of micro-holes will be needed to investigate the effect of probing repeatability due to the bottom of the blind hole.

Data availability statement

The original contributions presented in the study are included in the article/Supplementary material, further inquiries can be directed to the corresponding author.

Author contributions

MA worked on data analysis of experimental results and writing the manuscript. SI worked on planning the research, conducting the experiments and writing the manuscript. DK worked on the development and experimentation of experimental equipment. KM advised on the development of the experimental equipment. KK calculated the measurement uncertainty.

Funding

This research was supported by the Japan Society for the Promotion of Science (JSPS) KAKENHI grant number (20K04195).

Acknowledgments

The micro-hole sample used in this research was prepared with the cooperation of the Mitsubishi Electric Corporation. The authors would like to thank Mr. Takanori Miyazaki, Mr. Kenji Ito, and Mr. Yukitoshi Kudo for their involvement in sample preparation.

Conflict of interest

The authors declare that the research was conducted in the absence of any commercial or financial relationships that could be construed as a potential conflict of interest.

Publisher's note

All claims expressed in this article are solely those of the authors and do not necessarily represent those of their affiliated organizations, or those of the publisher, the editors and the reviewers. Any product that may be evaluated in this article, or claim that may be made by its manufacturer, is not guaranteed or endorsed by the publisher.

References

Arab, J., Kannojia, H. K., and Dixit, P. (2019). Effect of tool electrode roughness on the geometric characteristics of through-holes formed by ECDM. *Precision Engineering* 60, 437–447. doi:10.1016/j.precisioneng.2019.09.008

Aziz, M., Ohnishi, O., and Onikura, H. (2012). Novel micro deep drilling using micro long flat drill with ultrasonic vibration. *Precision Engineering* 36, 168–174. doi:10.1016/j.precisioneng.2011.07.010

Bos, E. J. C. (2011). Aspects of tactile probing on the micro scale. *Precision Engineering* 35, 228–240. doi:10.1016/j.precisioneng.2010.09.010

Cai, Y., Chang, W., Luo, X., Sousa, A. M. L., Lau, K. H. A., and Qin, Y. (2018). Superhydrophobic structures on 316L stainless steel surfaces machined by nanosecond pulsed laser. *Precision Engineering* 52, 266–275. doi:10.1016/j.precisioneng.2018.01.004

Chen, Y. L., Ito, S., Kikuchi, H., Kobayashi, R., Shimizu, Y., and Gao, W. (2016). On-line qualification of a micro probing system for precision length measurement of micro-features on precision parts. *Measurement Science and Technology* 27, 074008. doi:10.1088/0957-0233/27/7/074008

Claverley, J. D., and Leach, R. K. (2015). A review of the existing performance verification infrastructure for micro-CMMs. *Precision Engineering* 39, 1–15. doi:10.1016/j.precisioneng.2014.06.006

Claverley, J. D., and Leach, R. K. (2010). A vibrating micro-scale CMM probe for measuring high aspect ratio structures. *Microsystem Technologies* 16, 1507–1512. doi:10.1007/s00542-009-0967-2

Dai, G., Xu, L., and Hahm, K. (2020). Accurate tip characterization in critical dimension atomic force microscopy. *Measurement Science and Technology* 31, 074011. doi:10.1088/1361-6501/ab7fd2

Elfurjani, S., Ko, J., and Jun, M. B. G., (2016). Micro-scale hole profile measurement using rotating wire probe and acoustic emission contact detection. *Measurement* 89, 215–222. doi:10.1016/j.measurement.2016.04.023

Goj, B., Dressler, L., and Hoffmann, M. (2014). Semi-contact measurements of three-dimensional surfaces utilizing a resonant uniaxial microprobe. *Measurement Science and Technology* 25, 064012. doi:10.1088/0957-0233/25/6/064012

Gupta, U., Nath, A. K., and Bandyopadhyay, P. P. (2016). Laser micro-hole drilling in thermal barrier coated nickel based superalloy. *IOP Conf. Ser. Mater. Sci. Eng.* 149, 012076. doi:10.1088/1757-899x/149/1/012076

Ito, S., Chen, Y. L., Shimizu, Y., Kikuchi, H., Gao, W., Takahashi, K., et al. (2016a). Uncertainty analysis of slot die coater gap width measurement by using a shear mode micro-probing system. *Precision Engineering* 43, 525–529. doi:10.1016/j.precisioneng.2015.09.016

Ito, S., Kikuchi, H., Chen, Y., Shimizu, Y., Gao, W., Takahashi, K., et al. (2016b). A micro-coordinate measurement machine (CMM) for large-scale dimensional measurement of micro-Slits. *Applied Science* 6 (5), 156. doi:10.3390/app6050156

Ito, S., Shima, Y., Kato, D., Matsumoto, K., and Kamiya, K. (2020). Development of a microprobing system for side wall detection based on local surface interaction force detection. *International Journal of Automation Technology* 14 (1), 91–98. doi:10.20965/ijat.2020.p0091

JCGM 100 (2008). in *Evaluation of Measurement Data—Guide to the Expression of Uncertainty in Measurement (GUM)* (Paris, France: Bureau International des Poids et Mesures).

Kao, C. C., and Shih, A. J. (2007). Form measurements of micro-holes. *Measurement Science and Technology* 18, 3603–3611. doi:10.1088/0957-0233/18/11/045

Krüger, O., Schöne, G., Wernicke, T., John, W., Würfl, J., and Tränkle, G. (2007). UV laser drilling of SiC for semiconductor device fabrication. *Journal of Physics: Conference Series* 59, 740–744. doi:10.1088/1742-6596/59/1/158

Li, R., Wang, P., Li, D., Fan, K., Liu, F., Chen, L., et al. (2018). Precision manufacturing of patterned beryllium bronze leaf springs via chemical etching. *Applied Sciences* 8, 1476. doi:10.3390/app8091476

Li, S., Wang, L., Li, G., Zhang, S., Wu, S., Qiao, J., et al. (2021). Small hole drilling of Ti–6Al–4V using ultrasonic-assisted plasma electric oxidation grinding. *Precision Engineering* 67, 189–198. doi:10.1016/j.precisioneng.2020.09.020

Marimuthu, S., Antar, J. M., and Dunleavey, J. (2019). Characteristics of micro-hole formation during fibre laser drilling of aerospace superalloy. *Precis. Eng.* 55, 339–348. doi:10.1016/j.precisioneng.2018.10.002

Masuzawa, T., Hamasaki, Y., and Fujino, M. (1993). Vibroscanning method for nondestructive measurement of small holes. *CIRP Annals - Manufacturing Technology* 42 (1), 589–592. doi:10.1016/s0007-8506(07)62516-5

Metz, D., Jantzen, S., Wessel, D., Mies, G., Lüdenbach, J., Stein, M., et al. (2019). Integration of an isotropic microprobe and a microenvironment into a conventional CMM. *Measurement Science and Technology* 30, 115007. doi:10.1088/1361-6501/ab2fda

Murakami, H., Katsuki, A., Sajima, T., and Suematsu, T. (2014). Study of a vibrating fiber probing system for 3-D micro-structures: Performance improvement. *Measurement Science and Technology* 25, 094010. doi:10.1088/0957-0233/25/9/094010

Saranya, S., and Sankar, A. R. (2018). Fabrication of precise micro-holes on quartz substrates with improved aspect ratio using a constant velocity-feed drilling technique of an ECDM process. *Journal of Micromechanics and Microengineering* 28, 125009. doi:10.1088/1361-6439/aae8f5

Sato, S., Hidai, H., Matsusaka, S., Chiba, A., and Morita, N. (2020). Drilling, bonding, and forming conductive path in the hole by laser percussion drilling. *Precision Engineering* 61, 147–151. doi:10.1016/j.precisioneng.2019.10.007

Song, W., Wang, S., Lu, Y., and Xia, Z. (2018). Tribological performance of microhole-textured carbide tool filled with CaF2. *Materials* 11 (9), 1643. doi:10.3390/ma11091643

Thalmann, R., Meli, F., and Küng, A. (2016). State of the art of tactile micro coordinate metrology. *Applied Science* 6 (5), 150. doi:10.3390/app6050150

Tong, H., Li, Y., Zhang, L., and Li, B. (2013). Mechanism design and process control of micro EDM for drilling spray holes of diesel injector nozzles. *Precision Engineering* 37, 213–221. doi:10.1016/j.precisioneng.2012.09.004

Weckenmann, A., Estler, T., Peggs, G., and McMurtry, D. (2004). Probing systems in dimensional metrology. *CIRP Annals - Manufacturing Technology* 53 (2), 657–684. doi:10.1016/s0007-8506(07)60034-1

Weckenmann, A., Peggs, G., and Hoffmann, J. (2006). Probing systems for dimensional micro- and nano-metrology. *Measurement Science and Technology* 17, 504–509. doi:10.1088/0957-0233/17/3/s08

Weckenmann, A., and Schuler, A. (2011). Application of modern high resolution tactile sensors for micro-objects. *International Journal of Precision Technology* 2 (2/3), 266–288. doi:10.1504/ijptech.2011.039463

Wilson, T. (1995). "The role of the pinhole in confocal imaging system," in *Handbook of biological confocal microscopy*. Editor J. B. Pawley (Boston, MA, USA: Springer), 167–182.